Parametric X-Ray Radiation along Relativistic Electron Velocity in Asymmetric Laue Geometry

S. V. Blazhevich[a] and A. V. Noskov[b, *]

[a] *Belgorod State University, Belgorod, 308015 Russia*

[b] *Belgorod University of Consumers' Cooperation, Belgorod, 308023 Russia*

**e-mail: noskovbupk@mail.ru*

Abstract—An analysis is presented of the parametric X-ray radiation emitted by a relativistic electron at a small angle to its velocity as it passes through a single-crystal plate in asymmetric Laue geometry (including symmetric geometry as a particular case). Expressions describing the spectral-angular distributions of parametric X-ray radiation, transition radiation, and their interference are obtained. The effect of asymmetry on the spectral-angular distributions is examined.

1. INTRODUCTION

When a fast charged particle passes through a perfect crystal, the virtual photons associated with its Coulomb field are scattered from a set of parallel atomic planes of the crystal, giving rise to parametric X-ray radiation (PXR) [1–3]. For a relativistic particle, the PXR theory predicts emission not only in the Bragg direction, but also along the particle velocity (forward parametric X-ray radiation, FPXR) [4–6]. The latter phenomenon is due to the contribution of dynamical diffraction effects to PXR. Experimental studies of FPXR were attempted in [7–11], but the first observation of FPXR was reported relatively recently in [10], where the contribution of transition radiation to the X-ray background near the Bragg frequency was suppressed by destructive interference between the transition radiation waves generated at the entrance and exit surfaces of the crystal plate. However, the presentation in [10] did not include any analysis of the narrow peak appearing in the transition radiation spectrum near the Bragg frequency because of dynamical effects [12], which could well be interpreted as an FPXR peak in an experimental study. In the experiment reported in [11], X-ray radiation from relativistic electrons passing through a thick single-crystal target was detected under FPXR generation conditions, but the desired reflex was barely observable against the background emission from electrons interacting with parts of the experimental setup. Thus, theoretical characterization of FPXR and finding optimal conditions for observation of this dynamical effect remain challenging tasks.

A detailed theoretical description of the dynamical phenomenon of FPXR and the accompanying background of transition radiation in symmetric geometry was given in [13–15]. A theoretical description of PXR and transition radiation (TR) in asymmetric geometry was given in [16–18], and FPXR in Bragg geometry was analyzed in [19]. Those studies demonstrated a strong dependence of the spectral-angular distributions associated with these radiation mechanisms on reflection asymmetry and revealed effects due to asymmetry.

In this paper, we analyze the forward parametric X-ray radiation emitted by a relativistic electron in the general case of asymmetric Laue geometry, when the diffracting planes make an arbitrary angle δ with the target surface. The two-beam approximation of dynamical diffraction theory [20] is used to derive expressions describing the spectral-angular distributions of FPXR and TR and the contribution resulting from their interference (denoted by superscript INT).

2. SPECTRAL-ANGULAR DISTRIBUTION

We analyze the radiation emitted by a relativistic electron passing through a crystal plate of thickness L with a constant velocity $\mathbf{v}$ (Fig. 1), using an equation for the Fourier transform of the electromagnetic field,

$$\mathbf{E}(\mathbf{k}, \omega) = \int dt d^3\mathbf{r}\mathbf{E}(\mathbf{r}, t)e^{i\omega t - i\mathbf{k}\cdot\mathbf{r}}. \quad (1)$$

Since the electromagnetic field associated with a relativistic particle can accurately be considered as transverse, both incident wave $\mathbf{E}_0(\mathbf{k}, \omega)$ and diffracted

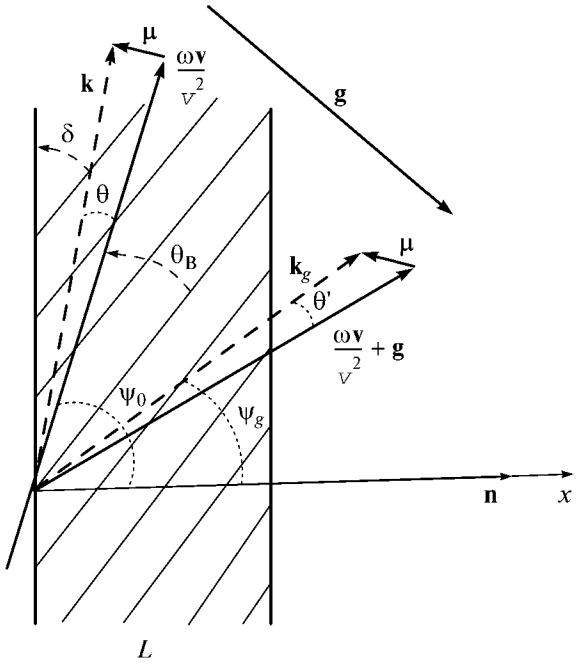

Fig. 1. Radiation geometry: θ' is the polar emission angle, θ_B is the Bragg angle (the angle between electron velocity **v** and diffracting atomic planes), δ is the angle between the crystal surface and the diffracting planes, **k** is the incident wavevector, and $\mathbf{k}_g = \mathbf{k} + \mathbf{g}$ is the diffracted wavevector.

wave $\mathbf{E}_g(\mathbf{k}, \omega)$ are determined by pairs of transverse polarization amplitudes:

$$\begin{aligned} \mathbf{E}_0(\mathbf{k}, \omega) &= E_0^{(1)}(\mathbf{k}, \omega)\mathbf{e}_0^{(1)} + E_0^{(2)}(\mathbf{k}, \omega)\mathbf{e}_0^{(2)}, \\ \mathbf{E}_g(\mathbf{k}, \omega) &= E_g^{(1)}(\mathbf{k}, \omega)\mathbf{e}_1^{(1)} + E_g^{(2)}(\mathbf{k}, \omega)\mathbf{e}_1^{(2)}. \end{aligned} \tag{2}$$

The unit polarization vectors $\mathbf{e}_0^{(1)}$, $\mathbf{e}_0^{(2)}$, $\mathbf{e}_1^{(1)}$, and $\mathbf{e}_1^{(2)}$ are defined as follows. The vectors $\mathbf{e}_0^{(1)}$ and $\mathbf{e}_0^{(2)}$ are perpendicular to **k** while the vectors $\mathbf{e}_1^{(1)}$ and $\mathbf{e}_1^{(2)}$ are perpendicular to $\mathbf{k}_g = \mathbf{k} + \mathbf{g}$, and the vectors $\mathbf{e}_0^{(2)}$ and $\mathbf{e}_1^{(2)}$ lie in the plane spanned by **k** and $\mathbf{k}_g$ (π-polarization) while $\mathbf{e}_0^{(1)}$ and $\mathbf{e}_1^{(1)}$ are perpendicular to that plane (σ-polarization). The reciprocal lattice vector **g** specifies a particular set of reflecting atomic planes of the crystal. In the two-beam approximation, the system of equations for the Fourier transform of the electromagnetic field is written as follows [21]:

$$\begin{aligned} &(\omega^2(1+\chi_0) - k^2)E_0^{(s)} + \omega^2\chi_{-g}C^{(s)}E_g^{(s)} \\ &\quad = 8\pi^2 ie\omega\theta v P^{(s)}\delta(\omega - \mathbf{k}\cdot\mathbf{v}), \\ &\omega^2\chi_g C^{(s)}E_0^{(s)} + (\omega^2(1+\chi_0) - k_g^2)E_g^{(s)} = 0, \end{aligned} \tag{3}$$

where χ_g and χ_{-g} are coefficients in the Fourier expansion of the dielectric susceptibility of the crystal in reciprocal lattice vectors **g**,

$$\begin{aligned} \chi(\omega, \mathbf{r}) &= \sum_g \chi_g(\omega)e^{i\mathbf{g}\cdot\mathbf{r}} \\ &= \sum_g (\chi_g'(\omega) + i\chi_g''(\omega))e^{i\mathbf{g}\cdot\mathbf{r}}. \end{aligned} \tag{4}$$

We consider a centrosymmetric crystal ($\chi_g = \chi_{-g}$) and use the following expressions for χ_g' and χ_g'' in (4):

$$\chi_g' = \chi_0' \frac{F(g)}{Z}\frac{S(\mathbf{g})}{N_0}\exp\left(-\frac{1}{2}g^2u_\tau^2\right), \tag{5a}$$

$$\chi_g'' = \chi_0''\exp\left(-\frac{1}{2}g^2u_\tau^2\right), \tag{5b}$$

where $\chi_0 = \chi_0' + i\chi_0''$ is the average dielectric susceptibility, $F(g)$ is the form factor for an atom containing Z electrons, $S(\mathbf{g})$ is the structure factor of an N_0-atom unit cell, and u_τ is the rms thermal vibration amplitude of atoms in the crystal. In the X-ray frequency range considered here, it holds that $\chi_g' < 0$ and $\chi_0' < 0$.

The parameters $C^{(s)}$ and $P^{(s)}$ in (3) are defined as

$$\begin{aligned} C^{(s)} &= \mathbf{e}_0^{(s)}\cdot\mathbf{e}_1^{(s)}, \quad C^{(1)} = 1, \\ C^{(2)} &= \cos 2\theta_B, \quad P^{(s)} = \mathbf{e}_0^{(s)}\left(\frac{\boldsymbol{\mu}}{\mu}\right), \\ P^{(1)} &= \sin\varphi, \quad P^{(2)} = \cos\varphi. \end{aligned} \tag{6}$$

Here, $\boldsymbol{\mu} = \mathbf{k} - \omega\mathbf{v}/v^2$ is the virtual photon momentum component perpendicular to the particle velocity **v** ($\mu = \omega\theta/v$, where $\theta \ll 1$ is the angle between **k** and **v**); the Bragg angle θ_B is defined as the angle between the electron velocity and a set of crystallographic planes; the azimuthal emission angle φ is measured from the plane spanned by **v** and **g**; and the reciprocal lattice vector magnitude is expressed as $g = 2\omega_B\sin\theta_B/v$, where ω_B is the Bragg frequency. We denote by θ the angle between vector $\omega\mathbf{v}/v^2$ and wavevector **k** of the incident wave and by θ' the angle between vector $\omega\mathbf{v}/v^2 + \mathbf{g}$ and wavevector $\mathbf{k}_g$ of the diffracted wave. Equations (3) with $s = 1$ and 2 describe σ- and π-polarized wave fields, respectively.

Combining Eqs. (3), we obtain a dispersion relation for X-rays in the crystal:

$$\begin{aligned} &(\omega^2(1+\chi_0) - k^2)(\omega^2(1+\chi_0) - k_g^2) \\ &\quad - \omega^4\chi_{-g}\chi_g C^{(s)^2} = 0. \end{aligned} \tag{7}$$

We analyze this relation by standard methods of dynamical diffraction theory [20].

We represent the x-components of **k** and $\mathbf{k}_g$ along the normal vector **n** to the crystal surface (see Fig. 1), as

$$k_x = \omega\cos\psi_0 + \frac{\omega\chi_0}{2\cos\psi_0} + \frac{\lambda_0}{\cos\psi_0}, \quad (8a)$$

$$k_{gx} = \omega\cos\psi_g + \frac{\omega\chi_0}{2\cos\psi_g} + \frac{\lambda_g}{\cos\psi_g}. \quad (8b)$$

We use a well-known relation between the dynamical corrections λ_0 and λ_g for X-rays [20],

$$\lambda_g = \frac{\omega\beta}{2} + \lambda_0\frac{\gamma_g}{\gamma_0}, \quad (9)$$

where

$$\beta = \alpha - \chi_0\left(1 - \frac{\gamma_g}{\gamma_0}\right), \quad \alpha = \frac{1}{\omega^2}(k_g^2 - k^2),$$

$$\gamma_0 = \cos\psi_0, \quad \gamma_g = \cos\psi_g,$$

ψ_0 is the angle between $\mathbf{k}$ and $\mathbf{n}$, and ψ_g is the angle between $\mathbf{k}_g$ and $\mathbf{n}$ (see Fig. 1). The magnitudes of $\mathbf{k}$ and $\mathbf{k}_g$ are

$$k = \omega\sqrt{1+\chi_0} + \lambda_0, \quad k_g = \omega\sqrt{1+\chi_0} + \lambda_g. \quad (10)$$

Substituting expressions (8) into Eq. (7), using (9), and noting that the wavevector components along the crystal surface are $k_{\parallel} \approx \omega\sin\psi_0$ and $k_{g\parallel} \approx \omega\sin\psi_g$, we find expressions for the dynamical corrections:

$$\lambda_g^{(1,2)} = \frac{\omega}{4}\left(\beta \pm \left(\beta^2 + 4\chi_g\chi_{-g}C^{(s)^2}\frac{\gamma_g}{\gamma_0}\right)^{1/2}\right), \quad (11a)$$

$$\lambda_0^{(1,2)} = \omega\frac{\gamma_0}{4\gamma_g} \times\left(-\beta \pm \left(\beta^2 + 4\chi_g\chi_{-g}C^{(s)^2}\frac{\gamma_g}{\gamma_0}\right)^{1/2}\right). \quad (11b)$$

The incident wave amplitude in the crystal obtained by solving Eqs. (3) is conveniently represented as

$$E_0^{(s)\mathrm{cr}} = \frac{8\pi^2 ie\nu\theta P^{(s)}}{\omega} \times\frac{-\omega^2\beta - 2\omega\gamma_g\lambda_0/\gamma_0}{4\gamma_g(\lambda_0 - \lambda_0^{(1)})(\lambda_0 - \lambda_0^{(2)})/\gamma_0}\delta(\lambda_0 - \lambda_0^*) + E_0^{(s)^{(1)}}\delta(\lambda_0 - \lambda_0^{(1)}) + E_0^{(s)^{(2)}}\delta(\lambda_0 - \lambda_0^{(2)}), \quad (12)$$

where $\lambda_0^* = \omega(\gamma^{-2} + \theta^2 - \chi_0)/2$, $\gamma = \sqrt{1-v^2}$ is the Lorentz factor of the particle, and $E_0^{(s)^{(1)}}$ and $E_0^{(s)^{(2)}}$ are the field amplitudes of real incident photons in the crystal.

The solution to Eqs. (3) for the field amplitude in vacuum at the entrance surface is

$$E_0^{(s)\mathrm{vacI}} = \frac{8\pi^2 ie\nu\theta P^{(s)}}{\omega}\frac{1}{-\chi_0 - 2\lambda_0/\omega} \times\delta(\lambda_0 - \lambda_0^*). \quad (13)$$

The field amplitude in vacuum at the exit surface is

$$E_0^{(s)\mathrm{vacII}} = \frac{8\pi^2 ie\nu\theta P^{(s)}}{\omega}\frac{1}{-\chi_0 - 2\lambda_0/\omega} \times\delta(\lambda_0 - \lambda_0^*) + E_0^{(s)\mathrm{rad}}\delta\left(\lambda_0 + \frac{\omega\chi_0}{2}\right), \quad (14)$$

where $E_0^{(s)\mathrm{rad}}$ is the field amplitude of the coherent radiation emitted along the electron velocity.

The second equation in (3) yields a relation between the diffracted and incident field amplitudes in the crystal:

$$E_0^{(s)\mathrm{cr}} = \frac{2\omega\lambda_g}{\omega^2\chi_g C^{(s)}}E_g^{(s)\mathrm{cr}}. \quad (15)$$

Using standard boundary conditions at the entrance and exit surfaces of the crystal plate,

$$\int E_0^{(s)\mathrm{vacI}}d\lambda_0 = \int E_0^{(s)\mathrm{cr}}d\lambda_0,$$

$$\int E_g^{(s)\mathrm{cr}}d\lambda_0 = 0, \quad (16)$$

$$\int E_0^{(s)\mathrm{cr}}e^{i\lambda_0 L/\gamma_0}d\lambda_0 = \int E_0^{(s)\mathrm{vacII}}e^{i\lambda_0 L/\gamma_0}d\lambda_0,$$

we obtain the radiation field amplitude

$$E^{(s)\mathrm{rad}} = -\frac{4\pi^2 ie\nu\theta P^{(s)}}{\omega}\exp\left(i\frac{\lambda_0^* + \omega\chi_0/2}{\gamma_0}L\right) \times\left[\left(1 - \beta\left(\beta^2 + 4\chi_g\chi_{-g}C^{(s)^2}\frac{\gamma_g}{\gamma_0}\right)^{-1/2}\right) \times\left(\frac{\omega}{-\omega\chi_0 - 2\lambda_0^*} + \frac{\omega}{2(\lambda_0^* - \lambda_0^{(2)})}\right) \times\left(1 - \exp\left(i\frac{\lambda_0^{(2)} - \lambda_0^*}{\gamma_0}L\right)\right) + \left(1 + \beta\left(\beta^2 + 4\chi_g\chi_{-g}C^{(s)^2}\frac{\gamma_g}{\gamma_0}\right)^{-1/2}\right) \times\left(\frac{\omega}{-\omega\chi_0 - 2\lambda_0^*} + \frac{\omega}{2(\lambda_0^* - \lambda_0^{(1)})}\right) \times\left(1 - \exp\left(i\frac{\lambda_0^{(1)} - \lambda_0^*}{\gamma_0}L\right)\right)\right]. \quad (17)$$

Expression (17) can be used to describe spectral and angular characteristics of the radiation.

Prior to analyzing spectral-angular characteristics, it should be noted that the total radiation yield combines the contributions of three radiation mechanisms: bremsstrahlung, transition radiation, and FPXR. The amplitude $E^{(s)\mathrm{rad}}$ contains FPXR and TR contributions. Since TR background is the main factor that complicates the observation and experimental study of FPXR, we represent the amplitude $E^{(s)\mathrm{rad}}$ given by (17) as the sum of FPXR and TR field ampli-

tudes to evaluate the contributions due to these mechanisms and their interference:

$$E_0^{(s)\mathrm{rad}} = E_0^{(s)\mathrm{FPXR}} + E_0^{(s)\mathrm{TR}}, \tag{18a}$$

$$E_0^{(s)\mathrm{FPXR}} = \frac{4\pi^2 ie\nu\theta P^{(s)}}{\omega}\exp\left(i\frac{\lambda_0^* + \omega\chi_0/2}{\gamma_0}L\right)$$
$$\times \frac{\omega^2\chi_g\chi_{-g}C^{(s)^2}}{2\sqrt{\beta^2 + 4\chi_g\chi_{-g}C^{(s)^2}\frac{\gamma_g}{\gamma_0}}}\frac{1}{\lambda_0^*}$$
$$\times\left[\frac{1-\exp\left(i\frac{\lambda_0^{(2)}-\lambda_0^*}{\gamma_0}\right)}{\lambda_0^*-\lambda_0^{(2)}}\right.$$
$$\left. - \frac{1-\exp\left(i\frac{\lambda_0^{(1)}-\lambda_0^*}{\gamma_0}\right)}{\lambda_0^*-\lambda_0^{(1)}}\right], \tag{18b}$$

$$E_0^{(s)\mathrm{TR}} = \frac{4\pi^2 ie\nu\theta P^{(s)}}{\omega}\exp\left(i\frac{\lambda_0^* + \omega\chi_0/2}{\gamma_0}L\right)$$
$$\times\left(\frac{\omega}{\omega\chi_0 + 2\lambda_0^*} - \frac{\omega}{2\lambda_0^*}\right)$$
$$\times\left[\left(1-\beta\left(\beta^2 + 4\chi_g\chi_{-g}C^{(s)^2}\frac{\gamma_g}{\gamma_0}\right)^{-1/2}\right)\right.$$
$$\times\left(1-\exp\left(i\frac{\lambda_0^{(2)}-\lambda_0^*}{\gamma_0}L\right)\right)$$
$$\left.+\left(1+\beta\left(\beta^2 + 4\chi_g\chi_{-g}C^{(s)^2}\frac{\gamma_g}{\gamma_0}\right)^{-1/2}\right)\right.$$
$$\left.\times\left(1-\exp\left(i\frac{\lambda_0^{(1)}-\lambda_0^*}{\gamma_0}L\right)\right)\right]. \tag{18c}$$

The first and second bracketed expressions in (18b) and (18c) represent two dispersion branches of X-rays generated in the crystal, referred to as branch 2 and branch 1 below.

In the analysis below, we use the following expressions for dynamical corrections (11):

$$\lambda_0^{(1,2)} = \frac{\omega|\chi_g'|C^{(s)}}{2\varepsilon}\left[-\xi^{(s)} + \frac{i\rho^{(s)}(1-\varepsilon)}{2}\right.$$
$$\left.\pm\left(\xi^{(s)^2} + \varepsilon - 2i\rho^{(s)}\left(\frac{1-\varepsilon}{2}\xi^{(s)} + \kappa^{(s)}\varepsilon\right)\right.\right.$$
$$\left.\left. - \rho^{(s)^2}\left(\frac{(1-\varepsilon)^2}{4} + \kappa^{(s)^2}\varepsilon\right)\right)^{1/2}\right], \tag{19a}$$

where

$$\xi^{(s)}(\omega) = \eta^{(s)}(\omega) + \frac{1-\varepsilon}{2\nu^{(s)}},$$

$$\eta^{(s)}(\omega) = \frac{\alpha}{2|\chi_g'|C^{(s)}} = \frac{2\sin^2\theta_B}{\nu^2|\chi_g'|C^{(s)}}$$
$$\times\left(1 - \frac{\omega(1-\theta\cos\varphi\cot\theta_B)}{\omega_B}\right), \tag{19b}$$

$$\varepsilon = \frac{\gamma_g}{\gamma_0} = \frac{\cos\psi_g}{\cos\psi_0}, \quad \nu^{(s)} = \frac{\chi_g'C^{(s)}}{\chi_0'},$$

$$\rho^{(s)} = \frac{\chi_0''}{|\chi_0'|C^{(s)}}, \quad \kappa^{(s)} = \frac{\chi_g''C^{(s)}}{\chi_0''}.$$

Since the inequality $2\sin^2\theta_B/\nu^2|\chi_g'|C^{(s)} \gg 1$ holds in the X-ray frequency range, $\eta^{(s)}(\omega)$ is a rapidly varying function of ω. Therefore, further analysis is greatly facilitated by using $\eta^{(s)}(\omega)$ as a frequency variable. Expression (19a) contains an important parameter ε, which quantifies the degree of asymmetry. In particular, $\varepsilon = 1$ and $\delta = \pi/2$ (the incident and diffracted wavevectors make equal angles with the plate surface) in the symmetric case, and $\varepsilon \neq 1$ and $\delta \neq \pi/2$ otherwise.

We represent the asymmetry ratio as

$$\varepsilon = \frac{\sin(\delta + \theta_B)}{\sin(\delta - \theta_B)}, \tag{20}$$

noting that the electron angle of incidence $\delta - \theta_B$ increases with decreasing ε and vice versa (see Fig. 2).

The parameter $\nu^{(s)}$ characterizes the reflecting power of a set of atomic planes as determined by the interference between waves scattered by atoms in different planes ($\nu^{(s)} \approx 1$ and 0 when the interference is constructive and destructive, respectively). Dynamical diffraction phenomena, such as FPXR, can be observed only when the interference is constructive.

The parameter $\rho^{(s)}$ is the ratio between the extinction length $L_{\mathrm{ext}}^{(s)} = 1/\omega|\chi_g'|C^{(s)}$ and the absorption length $L_{\mathrm{abs}} = 1/\omega\chi_0''$ for X-rays in the crystal. Note that the energy of the primary wave is completely transferred to the secondary wave propagating in the Bragg direction at the depth equal to the extinction length.

The parameter $\kappa^{(s)}$ quantifies the anomalous transmission effect (Borrmann effect) [22] for X-rays passing through a crystal. The absorption coefficients for the two branches of real emitted X-rays are [20]

$$\mu = \omega\chi_0''(1 \pm \kappa^{(s)}). \tag{21}$$

According to this formula, a necessary condition for anomalous transmission of branch 2 is $\kappa^{(s)} \approx 1$, which corresponds to anomalously strong absorption of branch 1.

The dynamical corrections $\lambda_0^{(1,2)}$ corresponding to the two branches of dispersion relation (7) depend not only on photon frequency and target properties, but also on ε. Thus, the dispersion of real photons in the crystal depends on asymmetry:

$$k^{(1,2)} = \omega\sqrt{1+\chi_0} + \lambda_0^{(1,2)}(\omega, \varepsilon). \tag{22}$$

The dispersion of virtual photons associated with the Coulomb field is described by the formula

$$k^* = \omega\sqrt{1+\chi_0} + \lambda_0^* = \omega + \frac{\omega}{2}(\theta^2 + \gamma^{-2}). \tag{23}$$

An FPXR reflex can be observed only if at least one denominator in the bracketed expression in (18b) vanishes:

$$\mathrm{Re}(\lambda_0^* - \lambda_0^{(1)}) = 0, \quad \mathrm{Re}(\lambda_0^* - \lambda_0^{(2)}) = 0. \tag{24}$$

Substituting (19a) into (18b) and (18c), we represent the FPXR and TR field amplitudes as

$$E_0^{(s)\mathrm{FPXR}} = \frac{4\pi^2 ie\,v\theta P^{(s)}}{\omega}\frac{\exp(i\omega(\gamma^{-2}+\theta^2)L/2\gamma_0)}{\gamma^{-2}+\theta^2-\chi_0}\frac{1}{\sqrt{\xi^{(s)^2}+\varepsilon}}$$
$$\times\left(\frac{1-\exp\left(-ib^{(s)}\left(\sigma^{(s)}+\dfrac{\xi^{(s)}+\sqrt{\xi^{(s)^2}+\varepsilon}}{\varepsilon}\right)-b^{(s)}\rho^{(s)}\Delta^{(2)}\right)}{\sigma^{(s)}+\dfrac{\xi^{(s)}+\sqrt{\xi^{(s)^2}+\varepsilon}}{\varepsilon}-i\rho^{(s)}\Delta^{(2)}}\right. \tag{25a}$$
$$\left.-\frac{1-\exp\left(-ib^{(s)}\left(\sigma^{(s)}+\dfrac{\xi^{(s)}-\sqrt{\xi^{(s)^2}+\varepsilon}}{\varepsilon}\right)-b^{(s)}\rho^{(s)}\Delta^{(1)}\right)}{\sigma^{(s)}+\dfrac{\xi^{(s)}-\sqrt{\xi^{(s)^2}+\varepsilon}}{\varepsilon}-i\rho^{(s)}\Delta^{(1)}}\right),$$

$$E_0^{(s)\mathrm{TR}} = \frac{4\pi^2 ie\,v\theta P^{(s)}}{\omega}\exp\left(i\frac{\omega(\gamma^{-2}+\theta^2)L}{2\gamma_0}\right)\left(\frac{1}{\gamma^{-2}+\theta^2}-\frac{1}{\gamma^{-2}+\theta^2-\chi_0}\right)\left[\left(1-\frac{\xi^{(s)}}{\sqrt{\xi^{(s)^2}+\varepsilon}}\right)\right.$$
$$\times\left(1-\exp\left(-ib^{(s)}\left(\sigma^{(s)}+\frac{\xi^{(s)}+\sqrt{\xi^{(s)^2}+\varepsilon}}{\varepsilon}\right)-b^{(s)}\rho^{(s)}\Delta^{(2)}\right)\right)+\left(1+\frac{\xi^{(s)}}{\sqrt{\xi^{(s)^2}+\varepsilon}}\right) \tag{25b}$$
$$\left.\times\left(1-\exp\left(-ib^{(s)}\left(\sigma^{(s)}+\frac{\xi^{(s)}-\sqrt{\xi^{(s)^2}+\varepsilon}}{\varepsilon}\right)-b^{(s)}\rho^{(s)}\Delta^{(1)}\right)\right)\right],$$

where

$$\Delta^{(2)} = \frac{\varepsilon+1}{2\varepsilon}+\frac{1-\varepsilon}{2\varepsilon}\frac{\xi^{(s)}}{\sqrt{\xi^{(s)^2}+\varepsilon}}+\frac{\kappa^{(s)}}{\sqrt{\xi^{(s)^2}+\varepsilon}},$$
$$\Delta^{(1)} = \frac{\varepsilon+1}{2\varepsilon}-\frac{1-\varepsilon}{2\varepsilon}\left(\frac{\xi^{(s)}}{\sqrt{\xi^{(s)^2}+\varepsilon}}-\frac{\kappa^{(s)}}{\sqrt{\xi^{(s)^2}+\varepsilon}},\right) \tag{26}$$
$$\sigma^{(s)} = \frac{1}{|\chi_g'|C^{(s)}}(\theta^2+\gamma^{-2}-\chi_0'),$$
$$b^{(s)} = \frac{\omega|\chi_g'|C^{(s)}}{2}\frac{L}{\gamma_0}.$$

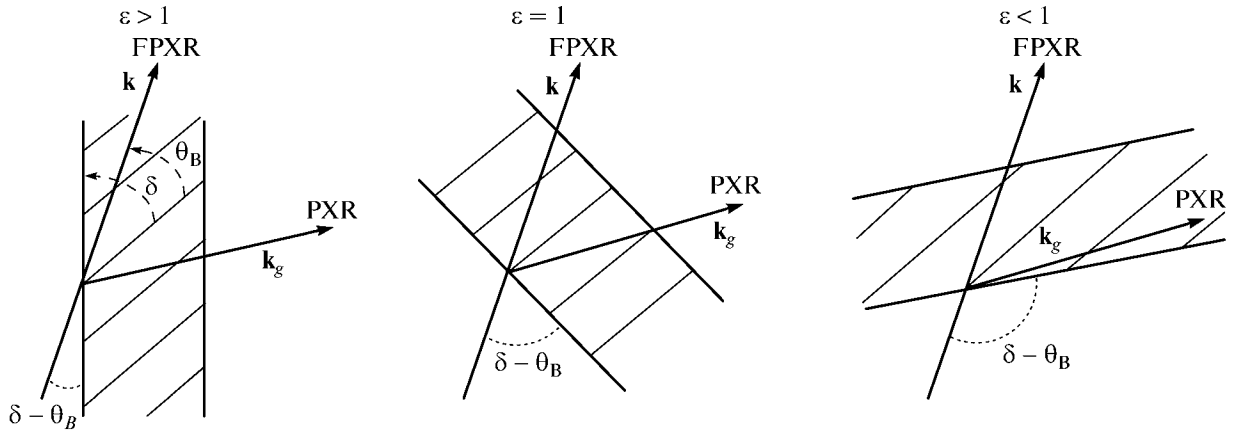

Fig. 2. Asymmetric ($\varepsilon > 1$, $\varepsilon < 1$) and symmetric ($\varepsilon = 1$) reflection geometries.

The parameter $b^{(s)}$ can be represented as

$$b^{(s)} = \frac{1}{2\sin(\delta - \theta_B)} \frac{L}{L_{ext}^{(s)}}; \tag{27}$$

i.e., $b^{(s)}$ is half the distance traveled by an electron in the plate, measured in units of extinction length.

The FPXR yield primarily comes from branch 1 in (19a), which corresponds to the second term in (25a), since only this term has a denominator with vanishing real part. Accordingly, the equation

$$\sigma^{(s)} + \frac{\xi^{(s)} - \sqrt{\xi^{(s)^2} + \varepsilon}}{\varepsilon} = 0 \tag{28}$$

determines the center frequency of the spectrum of FPXR photons emitted at a particular observation angle.

Substituting (18a), (25a), and (25b) into a well-known expression for the spectral-angular density of X-ray radiation [21],

$$\omega \frac{d^2 N}{d\omega d\Omega} = \omega^2 (2\pi)^{-6} \sum_{s=1}^{2} \left| E_0^{(s)\text{rad}} \right|^2, \tag{29}$$

we find the contributions to the spectral-angular density due to FPXR, TR, and their interference:

$$\omega \frac{d^2 N^{(s)\text{FPXR}}}{d\omega d\Omega} = \frac{e^2}{4\pi^2} P^{(s)^2} \times \frac{\theta^2}{(\theta^2 + \gamma^{-2} - \chi_0')^2} R^{(s)\text{FPXR}}, \tag{30a}$$

$$R^{(s)\text{FPXR}} = \frac{1}{\xi^{(s)^2} + \varepsilon}$$

$$\times \left[1 + \exp(-2b^{(s)}\rho^{(s)}\Delta^{(1)}) - 2\exp(-b^{(s)}\rho^{(s)}\Delta^{(1)}) \times \cos\left(b^{(s)} \left(\sigma^{(s)} + \frac{\xi^{(s)} - \sqrt{\xi^{(s)^2} + \varepsilon}}{\varepsilon} \right) \right) \right] \tag{30b}$$

$$\times \left[\left(\sigma^{(s)} + \frac{\xi^{(s)} - \sqrt{\xi^{(s)^2} + \varepsilon}}{\varepsilon} \right)^2 + (\rho^{(s)}\Delta^{(1)})^2 \right]^{-1},$$

$$\omega \frac{d^2 N^{(s)\text{TR}}}{d\omega d\Omega} = \frac{e^2}{4\pi^2} P^{(s)^2} \theta^2 \times \left(\frac{1}{\theta^2 + \gamma^{-2}} - \frac{1}{\theta^2 + \gamma^{-2} - \chi_0'} \right)^2 R^{(s)\text{TR}}, \tag{31a}$$

$$R^{(s)\text{TR}} = \left(1 - \frac{\xi^{(s)}}{\sqrt{\xi^{(s)^2} + \varepsilon}} \right)^2$$

$$\times \left(1 + \exp(-2b^{(s)}\rho^{(s)}\Delta^{(2)}) - 2\exp(-b^{(s)}\rho^{(s)}\Delta^{(2)}) \times \cos\left(b^{(s)} \left(\sigma^{(s)} + \frac{\xi^{(s)} + \sqrt{\xi^{(s)^2} + \varepsilon}}{\varepsilon} \right) \right) \right)$$

$$+ \left(1 + \frac{\xi^{(s)}}{\sqrt{\xi^{(s)^2} + \varepsilon}} \right)^2$$

$$\times \left(1 + \exp(-2b^{(s)}\rho^{(s)}\Delta^{(1)}) - 2\exp(-b^{(s)}\rho^{(s)}\Delta^{(1)}) \times \cos\left(b^{(s)} \left(\sigma^{(s)} + \frac{\xi^{(s)} - \sqrt{\xi^{(s)^2} + \varepsilon}}{\varepsilon} \right) \right) \right) \tag{31b}$$

$$+\frac{2\varepsilon}{\xi^{(s)2}+\varepsilon}\left[1+\exp\left(-b^{(s)}\rho^{(s)}\frac{\varepsilon+1}{\varepsilon}\right)\right.$$
$$\times\cos\left(\frac{2b^{(s)}\sqrt{\xi^{(s)2}+\varepsilon}}{\varepsilon}\right)-\exp(-b^{(s)}\rho^{(s)}\Delta^{(2)})$$
$$\left.\times\cos\left(b^{(s)}\left(\sigma^{(s)}+\frac{\xi^{(s)}-\sqrt{\xi^{(s)2}+\varepsilon}}{\varepsilon}\right)\right)\right]$$
$$-\exp(-b^{(s)}\rho^{(s)}\Delta^{(1)})$$
$$\times\cos\left(b^{(s)}\left(\sigma^{(s)}+\frac{\xi^{(s)}-\sqrt{\xi^{(s)2}+\varepsilon}}{\varepsilon}\right)\right)\Bigg],$$

$$\omega\frac{d^2N^{(s)\mathrm{INT}}}{d\omega d\Omega}=\frac{e^2}{4\pi^2}P^{(s)2}\theta^2$$
$$\times\left(\frac{1}{\theta^2+\gamma^{-2}}-\frac{1}{\theta^2+\gamma^{-2}-\chi_0'}\right)\qquad(32a)$$
$$\times\frac{1}{\theta^2+\gamma^{-2}-\chi_0'}R^{(s)\mathrm{INT}},$$

$$R^{(s)\mathrm{INT}}=-\frac{2}{\sqrt{\xi^{(s)2}+\varepsilon}}\mathrm{Re}\left(\frac{1-\exp\left(-ib^{(s)}\left(\sigma^{(s)}+\frac{\xi^{(s)}-\sqrt{\xi^{(s)2}+\varepsilon}}{\varepsilon}\right)-b^{(s)}\rho^{(s)}\Delta^{(1)}\right)}{\sigma^{(s)}+\frac{\xi^{(s)}-\sqrt{\xi^{(s)2}+\varepsilon}}{\varepsilon}-i\rho^{(s)}\Delta^{(1)}}\right.$$
$$\times\left(\left(1-\frac{\xi^{(s)}}{\sqrt{\xi^{(s)2}+\varepsilon}}\right)\left(1-\exp\left(ib^{(s)}\left(\sigma^{(s)}+\frac{\xi^{(s)}+\sqrt{\xi^{(s)2}+\varepsilon}}{\varepsilon}\right)-b^{(s)}\rho^{(s)}\Delta^{(2)}\right)\right)\right.\qquad(32b)$$
$$\left.\left.+\left(1+\frac{\xi^{(s)}}{\sqrt{\xi^{(s)2}+\varepsilon}}\right)\left(1-\exp\left(ib^{(s)}\left(\sigma^{(s)}+\frac{\xi^{(s)}-\sqrt{\xi^{(s)2}+\varepsilon}}{\varepsilon}\right)-b^{(s)}\rho^{(s)}\Delta^{(1)}\right)\right)\right)\right).$$

Expressions (30)–(32) are the main result of this study. They are obtained in the two-beam approximation of dynamical diffraction theory for an arbitrary orientation of the diffracting planes with respect to the surface of an absorbing crystal. In the particular case of symmetric geometry, when the diffracting planes are perpendicular to the surface ($\varepsilon = 1$), expressions (30)–(32) reduce to those obtained in [15].

In what follows, we analyze the effect of asymmetry on spectral-angular characteristics of radiation.

3. FPXR FROM A THIN TARGET

Suppose that the target is sufficiently thin that $b^{(s)}\rho^{(s)} \ll 1$; i.e., absorption is negligible. As a condition facilitating the observation of dynamical effects, we consider a plate whose thickness is such that the distance traveled by an electron in the plate, $L/\sin(\delta - \theta_B)$, far exceeds the extinction length for X-rays propagating in the crystal, $L_{\mathrm{ext}}^{(s)} = 1/\omega|\chi_g'|C^{(s)}$; i.e., $b^{(s)} \gg 1$ according to (27).

The spectral-angular distribution of the FPXR yield from a thin crystal follows from expression (30b):

$$\omega\frac{d^2N^{(s)\mathrm{FPXR}}}{d\omega d\Omega}=\frac{e^2}{4\pi^2}\frac{P^{(s)2}}{|\chi_0'|}\frac{\theta^2}{|\chi_0'|}$$
$$\times\left(\frac{\theta^2}{|\chi_0'|}+\frac{1}{\gamma^2|\chi_0'|}+1\right)^{-2}R^{(s)\mathrm{FPXR}},\qquad(33a)$$

$$R^{(s)\mathrm{FPXR}}=\frac{4}{\xi^{(s)2}+\varepsilon}$$
$$\times\left(\sigma^{(s)}+\frac{\xi^{(s)}-\sqrt{\xi^{(s)2}+\varepsilon}}{\varepsilon}\right)^{-2}\qquad(33b)$$
$$\times\sin^2\left(\frac{b^{(s)}}{2}\left(\sigma^{(s)}+\frac{\xi^{(s)}-\sqrt{\xi^{(s)2}+\varepsilon}}{\varepsilon}\right)\right),$$

where

$$\sigma^{(s)}=\frac{1}{\nu^{(s)}}\left(\frac{\theta^2}{|\chi_0'|}+\frac{1}{\gamma^2|\chi_0'|}+1\right),$$
$$\xi^{(s)}(\omega)=\eta^{(s)}(\omega)+\frac{1-\varepsilon}{2\nu^{(s)}}.$$

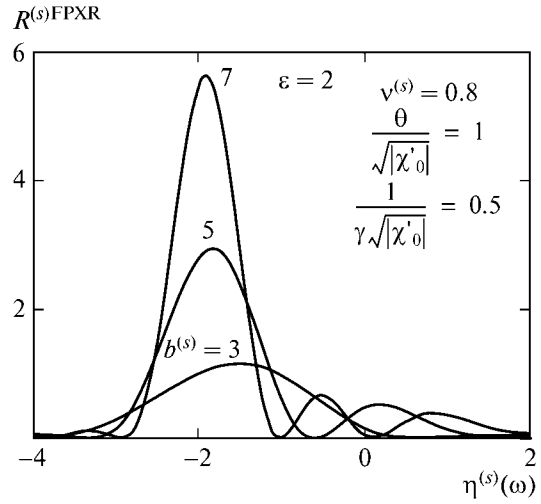

Fig. 3. Variation of FPXR spectrum with distance traveled by a particle in the target.

The curves of (33b) shown in Fig. 3 demonstrate that the height of the FPXR intensity peak increases with crystal thickness L, while its spectral width decreases. A remarkable property of FPXR is associated with the reflection asymmetry of the field generated by a relativistic electron: according to Fig. 4, the peak intensity of the FPXR spectrum also significantly increases with decreasing ε, while its width increases. Note that this property is demonstrated here by using the curves calculated for several values of ε and constant θ_B and $b^{(s)}$ (distance traveled by an electron in the plate).

To examine the effect of asymmetry on the angular density of PXR, we integrate (33a) with respect to the frequency variable $\eta^{(s)}(\omega)$:

$$\frac{dN^{(s)\mathrm{FPXR}}}{d\Omega} = \frac{e^2\nu^{(s)}P^{(s)^2}}{8\pi^2\sin^2\theta_B}F^{(s)\mathrm{FPXR}}, \qquad (34a)$$

$$F^{(s)\mathrm{FPXR}} = \frac{\theta^2}{|\chi'_0|}\left(\frac{\theta^2}{|\chi'_0|} + \frac{1}{\gamma^2|\chi'_0|} + 1\right)^{-2} \times \int_{-\infty}^{\infty} R^{(s)\mathrm{FPXR}}\, d\eta^{(s)}. \qquad (34b)$$

The curves of (34b) shown in Fig. 5 for several values of ε demonstrate that the maximum angular density considerably increases with decreasing asymmetry ratio. Thus, when θ_B and normalized distance $2b^{(s)}$ traveled by an electron in the crystal plate are held constant, both spectral peak intensity and angular density of FPXR strongly depend on the angle δ between the target surface and the set of diffracting atomic planes.

4. ANALYSIS OF TR CONTRIBUTION TO RADIATION YIELD AND EFFECT OF INTERFERENCE BETWEEN FPXR AND TR

Since FPXR can be observed experimentally only against a background of transition radiation, both the contribution of TR and the effect of interference between FPXR and TR must be analyzed. Using (31b), we obtain the following expression for the spectral-angular distribution of TR, valid in the case of a thin crystal:

$$\omega\frac{d^2N^{(s)\mathrm{TR}}}{d\omega d\Omega} = \frac{e^2}{4\pi^2}\frac{P^{(s)^2}}{|\chi'_0|}\frac{\theta^2}{|\chi'_0|} \times \left(\frac{\theta^2}{|\chi'_0|} + \frac{1}{\gamma^2|\chi'_0|} + 1\right)^{-2} \qquad (35a)$$

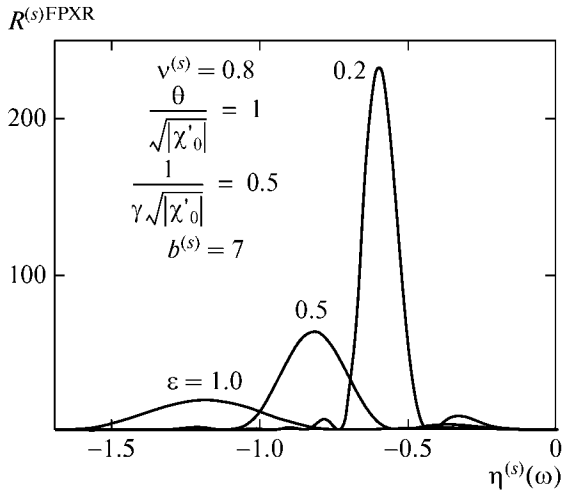

Fig. 4. Variation of FPXR spectrum with asymmetry.

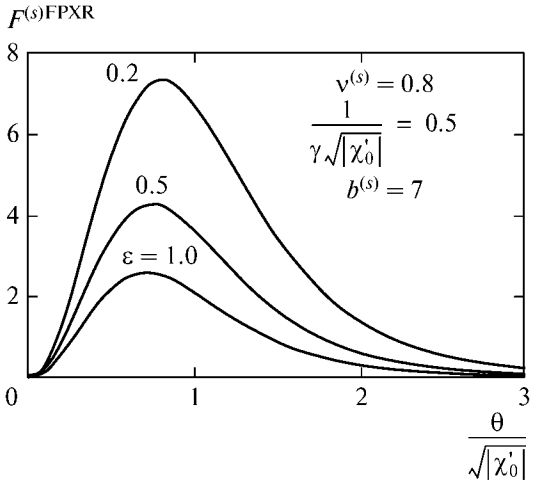

Fig. 5. Variation of FPXR angular density with asymmetry.

$$\times\left(\frac{\theta^2}{|\chi_0'|}+\frac{1}{\gamma^2|\chi_0'|}\right)^{-2}R^{(s)\mathrm{TR}},$$

$$R^{(s)\mathrm{TR}}=4\left(1-\frac{\xi^{(s)}}{\sqrt{\xi^{(s)^2}+\varepsilon}}\right)^2$$

$$\times\sin^2\left(\frac{b^{(s)}}{2}\left(\sigma^{(s)}+\frac{\xi^{(s)}+\sqrt{\xi^{(s)^2}+\varepsilon}}{\varepsilon}\right)\right)$$

$$+4\left(1+\frac{\xi^{(s)}}{\sqrt{\xi^{(s)^2}+\varepsilon}}\right)^2$$

$$\times\sin^2\left(\frac{b^{(s)}}{2}\left(\sigma^{(s)}+\frac{\xi^{(s)}-\sqrt{\xi^{(s)^2}+\varepsilon}}{\varepsilon}\right)\right) \qquad (35b)$$

$$+\frac{4\varepsilon}{\xi^{(s)^2}+\varepsilon}\left[\cos^2\left(\frac{b^{(s)}\sqrt{\xi^{(s)^2}+\varepsilon}}{\varepsilon}\right)\right.$$

$$-\cos\left(b^{(s)}\left(\sigma^{(s)}+\frac{\xi^{(s)}}{\varepsilon}\right)\right)$$

$$\left.\times\cos\left(b^{(s)}\left(\frac{\sqrt{\xi^{(s)^2}+\varepsilon}}{\varepsilon}\right)\right)\right].$$

Expression (35b) describes the spectrum of the transition radiation generated at the entrance and exit surfaces of the target. The first and second terms here correspond to branches 2 and 1, respectively; the last term, to interference between them.

Spectral distribution (35b) substantially differs from the conventional TR generated in an amorphous plate of the same thickness L. The difference is due to dynamical diffraction effects and is confined to a neighborhood of the Bragg frequency ω_B. Outside this neighborhood (when $|\xi^{(s)}| \gg \varepsilon$), the function $R^{(s)\mathrm{TR}}$ is given by the well-known expression

$$R^{(s)\mathrm{TR}}\approx 16\sin^2\left(\frac{b^{(s)}\sigma^{(s)}}{2}\right)$$

$$\equiv 16\sin^2\left(\frac{\omega L_e}{4}(\theta^2+\gamma^{-2}-\chi_0')\right) \qquad (36)$$

describing the interference between the TR waves generated at the entrance and exit surfaces, where L_e is the distance traveled by an electron in the plate.

According to (36), the contribution of normal TR to the total radiation yield is suppressed by interference effects near the Bragg frequency, where the FPXR peak is observed, if

$$\frac{b^{(s)}\sigma^{(s)}}{2}=\pi n,\quad n=0,\pm1,\ldots. \qquad (37)$$

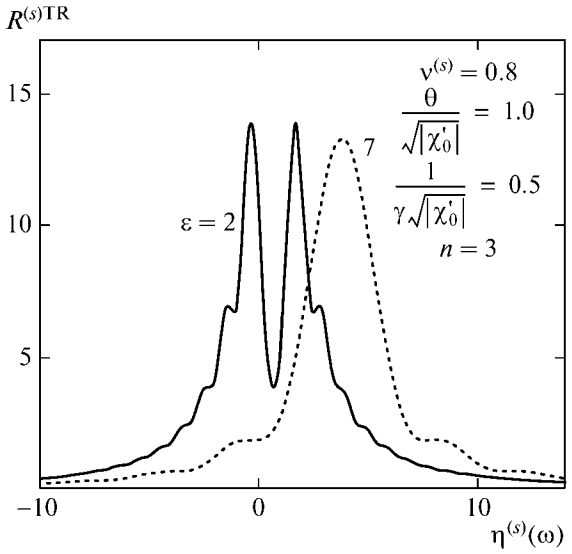

Fig. 6. Variation of TR spectrum with asymmetry (parameter ε).

Figure 6 shows the curves of $R^{(s)\mathrm{TR}}$ calculated by using formula (35b) for several values of ε and constant $\nu^{(s)}$ and $1/\gamma^2|\chi_0'|$, with parameter $b^{(s)}$ and observation angle θ satisfying resonance condition (37) for $n = 3$. It is clear from Fig. 6 that the shape of the TR peak varies with the asymmetry ratio. This is explained by the variation of the interference term in (35b) with the asymmetry-dependent relative phase between the transition radiation wave generated at the entrance surface and dynamically diffracted inside the crystal and the TR wave generated at the exit surface.

The angular distributions of TR and FPXR can be distinguished when the energy of the emitting particle is sufficiently high that $\gamma^2|\chi_0'| \gg 1$. Indeed, the maximum point of the TR angular distribution lies in the vicinity of $\theta \approx \gamma^{-1}$ according to expression (35a), whereas FPXR is concentrated around $\theta \sim \sqrt{|\chi_0'|} \gg \gamma^{-1}$ (see Fig. 5). The relative contributions of FPXR and TR to collimated radiation strongly depend on the observation angle θ. They are evaluated by using the following expressions derived from (32a) and (32b), respectively, to describe the interference between FPXR and TR in a thin crystal:

$$\omega\frac{d^2N^{(s)\mathrm{INT}}}{d\omega d\Omega}=\frac{e^2}{4\pi^2}\frac{P^{(s)^2}}{|\chi_0'|}\frac{\theta^2}{|\chi_0'|}$$

$$\times\left(\frac{\theta^2}{|\chi_0'|}+\frac{1}{\gamma^2|\chi_0'|}+1\right)^{-2} \qquad (38a)$$

$$\times\left(\frac{\theta^2}{|\chi_0'|}+\frac{1}{\gamma^2|\chi_0'|}\right)^{-1}R^{(s)\mathrm{INT}},$$

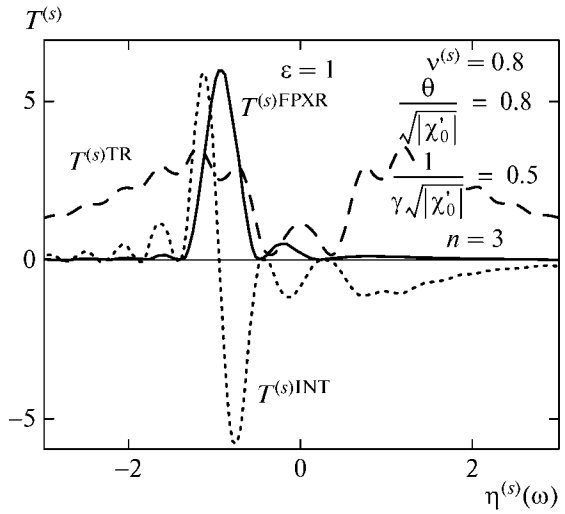

Fig. 7. Relative contributions of FPXR, TR, and their interference (INT) to the total radiation yield in symmetric geometry ($\varepsilon = 1$).

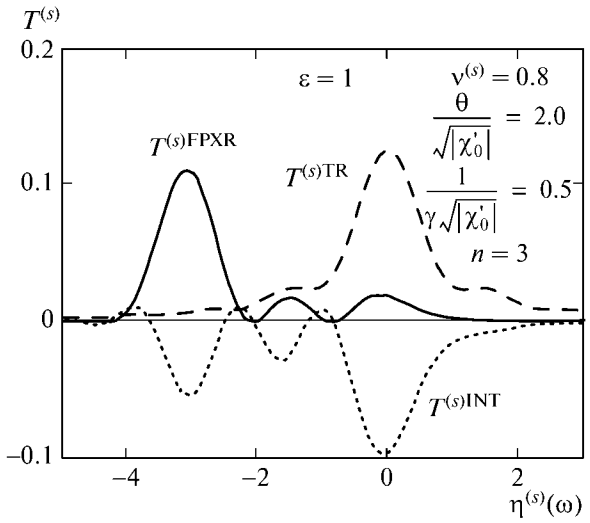

Fig. 8. Same as Fig. 7, but for a larger observation angle θ.

$$R^{(s)\mathrm{INT}} = -4\left(\xi^{(s)^2} + \varepsilon\right)^{-1/2} \times \left(\sigma^{(s)} + \frac{\xi^{(s)} - \sqrt{\xi^{(s)^2} + \varepsilon}}{\varepsilon}\right)^{-1} \times \left[\left(1 - \frac{\xi^{(s)}}{\sqrt{\xi^{(s)^2} + \varepsilon}}\right)\left(\cos^2\left(\frac{b^{(s)}\sqrt{\xi^{(s)^2} + \varepsilon}}{\varepsilon}\right)\right.\right. - \cos\left(\frac{b^{(s)}\sqrt{\xi^{(s)^2} + \varepsilon}}{\varepsilon}\right)\cos\left(b^{(s)}\left(\sigma^{(s)} + \frac{\xi^{(s)}}{\varepsilon}\right)\right)\Bigg) + 2\left(1 + \frac{\xi^{(s)}}{\sqrt{\xi^{(s)^2} + \varepsilon}}\right) \times \left.\sin^2\left(\frac{b^{(s)}}{2}\left(\sigma^{(s)} + \frac{\xi^{(s)} - \sqrt{\xi^{(s)^2} + \varepsilon}}{\varepsilon}\right)\right)\right]. \quad (38b)$$

The relative contributions of FPXR, TR, and their interference to the total radiation yield are conveniently analyzed by representing expressions (33), (35), and (38) as follows:

$$\omega\frac{d^2N^{(s)\mathrm{FPXR}}}{d\omega d\Omega} = \frac{e^2}{4\pi^2}\frac{P^{(s)^2}}{|\chi_0'|}T^{(s)\mathrm{FPXR}},$$

$$T^{(s)\mathrm{FPXR}} = \frac{\theta^2}{|\chi_0'|}\left(\frac{\theta^2}{|\chi_0'|} + \frac{1}{\gamma^2|\chi_0'|} + 1\right)^{-2} R^{(s)\mathrm{FPXR}}, \quad (39a)$$

$$\omega\frac{d^2N^{(s)\mathrm{TR}}}{d\omega d\Omega} = \frac{e^2}{4\pi^2}\frac{P^{(s)^2}}{|\chi_0'|}T^{(s)\mathrm{TR}},$$

$$T^{(s)\mathrm{TR}} = \frac{\theta^2}{|\chi_0'|}\left(\frac{\theta^2}{|\chi_0'|} + \frac{1}{\gamma^2|\chi_0'|} + 1\right)^{-2} \times \left(\frac{\theta^2}{|\chi_0'|} + \frac{1}{\gamma^2|\chi_0'|}\right)^{-2} R^{(s)\mathrm{TR}}, \quad (39b)$$

$$\omega\frac{d^2N^{(s)\mathrm{INT}}}{d\omega d\Omega} = \frac{e^2}{4\pi^2}\frac{P^{(s)^2}}{|\chi_0'|}T^{(s)\mathrm{INT}},$$

$$T^{(s)\mathrm{INT}} = \frac{\theta^2}{|\chi_0'|}\left(\frac{\theta^2}{|\chi_0'|} + \frac{1}{\gamma^2|\chi_0'|} + 1\right)^{-2} \times \left(\frac{\theta^2}{|\chi_0'|} + \frac{1}{\gamma^2|\chi_0'|}\right)^{-1} R^{(s)\mathrm{INT}}. \quad (39c)$$

Figures 7 and 8 show the spectral-angular distributions of TR, FPXR, and their interference calculated by formulas (39) under condition (37) for several observation angles in symmetric geometry ($\varepsilon = 1$). Note that both TR and FPXR peaks have widths of only a few electronvolts. The curves demonstrate a strong effect of the interference between FPXR and TR on the total radiation spectrum. According to Fig. 7, the narrow peak observed at small observation angles is mainly due to transition radiation. It is clear from Fig. 8 that the relative contribution of PXR increases with θ, whereas the total radiation yield drastically decreases. It should be noted that, according to Fig. 8, interference can substantially reduce the net contribution of TR to the total spectrum.

With decreasing ε, the contribution of TR to the total radiation yield, as compared to the FPXR contribution (Fig. 4), changes insignificantly (Fig. 6). For

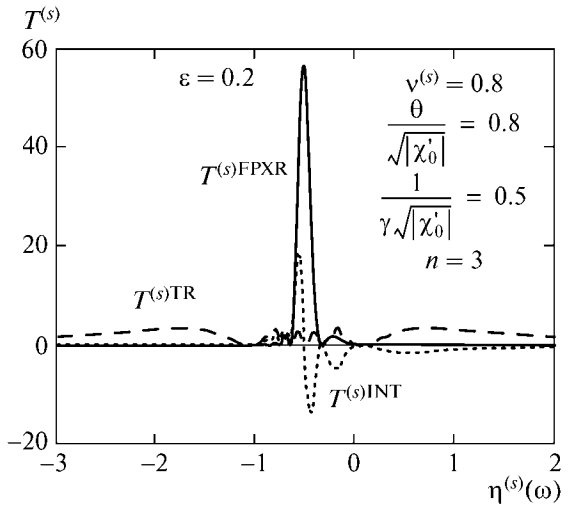

Fig. 9. Relative contributions of FPXR, TR, and their interference (INT) to the total radiation yield in asymmetric geometry. The distance traveled by an electron is as in Fig. 7.

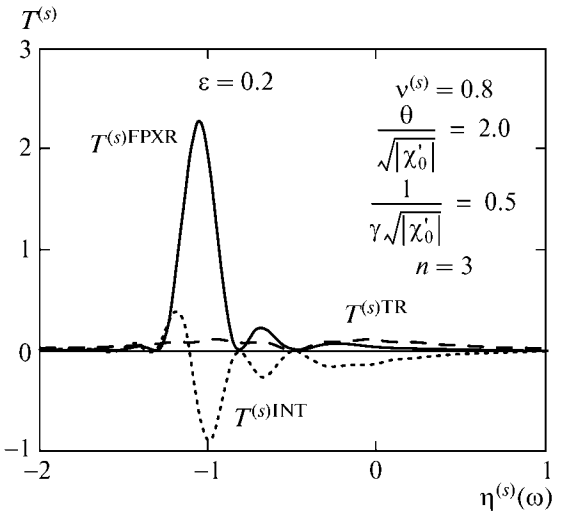

Fig. 10. Same as Fig. 9, but for a larger observation angle θ.

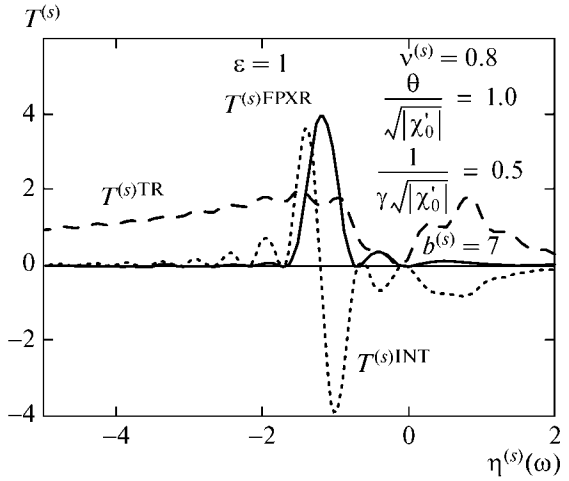

Fig. 11. Relative contributions of FPXR, TR, and their interference (INT) to the total radiation yield in symmetric geometry when condition (37) is violated.

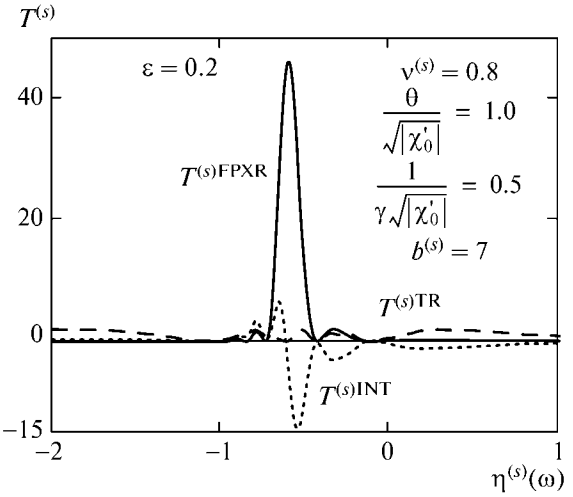

Fig. 12. Same as Fig. 11, but in asymmetric geometry. The FPXR contribution is dominant.

this reason, it is interesting to examine the curves plotted in Figs. 9 and 10 for a relatively large asymmetry and all other parameters as in Figs. 7 and 8. We see that the relative contribution of FPXR to the total radiation yield increases with asymmetry, becoming dominant at large observation angles, while interference remains significant.

Since TR suppression condition (37) is difficult to achieve in a real experiment, it is also interesting to compare the contributions of different radiation mechanisms for a crystal plate of arbitrary thickness. Figures 11 and 12 show curves calculated by using formulas (39). It is clear that the net contribution of FPXR to the total spectrum is negligible in symmetric geometry (see Fig. 11) and dominant when the asymmetry ratio is relatively large (see Fig. 12).

Thus, the dynamical phenomenon of FPXR is most clearly observed against the background of transition radiation when the target is a crystal cut as shown in the right panel of Fig. 2 ($\varepsilon < 1$).

5. CONCLUSIONS

The two-beam approximation of dynamical diffraction theory [20] is used to derive analytical expressions for the spectral-angular distribution of the coherent X-ray radiation emitted by a relativistic electron passing through a single-crystal plate along its

velocity in asymmetric Laue geometry, including the contributions of parametric X-ray radiation along the electron velocity (FPXR), transition radiation (TR), and their interference. It is shown that a decrease in asymmetry ratio (see Fig. 2) causes a significant increase in both spectral peak intensity and angular density of FPXR. It is also shown that variation in asymmetry changes the shape of the transition radiation peak by changing the relative phase between the TR wave generated at the entrance surface of crystal plate and dynamically diffracted inside the crystal and the TR wave generated at the exit surface of the target. An analysis is presented of the relative contributions of FPXR and TR to the total radiation yield and the effect of interference between these mechanisms. It is shown that the relative contribution of FPXR to the total radiation yield increases with decreasing asymmetry ratio at both large and small observation angles, becoming dominant when a certain degree of asymmetry is reached.

REFERENCES

1. M. L. Ter-Mikaelyan, *High-Energy Electromagnetic Processes in Condensed Media* (Academy of Sciences ArmSSR, Erevan, 1969; Wiley, New York, 1972), p. 459.
2. G. M. Garibyan and Yang Shi, Zh. Éksp. Teor. Fiz. **61**, 930 (1971) [Sov. Phys. JETP **34**, 495 (1971)].
3. V. G. Baryshevskiĭ and I. D. Feranchuk, Zh. Éksp. Teor. Fiz. **61**, 944 (1971) [Sov. Phys. JETP **34**, 502 (1971)].
4. G. M. Garibyan and Yang Shi, Zh. Éksp. Teor. Fiz. **63** (4), 1198 (1972) [Sov. Phys. JETP **36** (4), 631 (1973)].
5. V. G. Baryshevsky and I. D. Feranchuk, Phys. Lett. A **57**, 183 (1976).
6. V. G. Baryshevsky and I. D. Feranchuk, J. Phys. (Paris) **44**, 913 (1983).
7. Luke C. L. Yuan, P. W. Alley, A. Bamberger, G. F. Dell, and H. Uto, Nucl. Instrum. Methods Phys. Res., Sect. A **234**, 426 (1985).
8. B. N. Kalinin, G. A. Naumenko, D. V. Padalko, A. P. Potylitsyn, and I. E. Vnukov, Nucl. Instrum. Methods Phys. Res., Sect. B **173**, 253 (2001).
9. G. Kube, C. Ay, H. Backe, N. Clawiter, M. El-Ghazaly, F. Hagenbuck, K.-H. Kaiser, O. Kettig, W. Lauth, H. Mannweiler, D. Schroff, Th. Walcher, and T. Weber, in *Abstracts of Papers of the Fifth International Symposium "Radiation from Relativistic Electrons in Periodic Structures," Lake Aya, Altai Mountains, Russia, September 10–14, 2001* (Lake Aya, 2001).
10. H. Backe, C. Ay, N. Clawiter, Th. Doerk, M. El-Ghazaly, K.-H. Kaiser, O. Kettig, G. Kube, F. Hagenbuck, W. Lauth, A. Rueda, A. Scharafutdinov, D. Schroff, and T. Weber, in *Proceedings of the International Symposium on Channeling–Bent–Crystals–Radiation Processes, Frankfurt-on-Main, Germany, 2003* (EP Systema Bt., Debrecen, Hungary, 2003), p. 41.
11. A. N. Aleĭnik, A. N. Baldin, E. A. Bogomazova, I. E. Vnukov, B. N. Kalinin, A. S. Kubankin, N. N. Nasonov, G. A. Naumenko, A. P. Potylitsyn, and A. F. Sharafutdinov, Pis'ma Zh. Éksp. Teor. Fiz. **80** (6), 447 (2004) [JETP Lett. **80** (6), 393 (2004)].
12. N. Imanishi, N. Nasonov, and K. Yajima, Nucl. Instrum. Methods Phys. Res., Sect. B **173**, 227 (2001).
13. A. S. Kubankin, N. N. Nasonov, V. I. Sergienko, and I. E. Vnukov, Nucl. Instrum. Methods Phys. Res., Sect. B **201**, 97 (2003).
14. N. Nasonov and A. Noskov, Nucl. Instrum. Methods Phys. Res., Sect. B **201**, 67 (2003).
15. A. Kubankin, N. Nasonov, and A. Noskov, in *Proceedings of the Seventh International Russian–Japanese Symposium "Interaction of Fast Charged Particles with Solids," Kyoto, Japan, November 24–30, 2002* (Kyoto, 2002), p. 217.
16. S. Blazhevich and A. Noskov, Nucl. Instrum. Methods Phys. Res., Sect. B **252**, 69 (2006).
17. S. V. Blazhevich and A. V. Noskov, Nucl. Instrum. Methods Phys. Res., Sect. B **266**, 3770 (2008).
18. S. V. Blazhevich and A. V. Noskov, Nucl. Instrum. Methods Phys. Res., Sect. B **266**, 3777 (2008).
19. C. V. Blazhevich and A. V. Noskov, Izv. Vyssh. Uchebn. Zaved., Fiz. **50** (6), 48 (2007) [Russ. Phys. J. **50** (6), 574 (2007)].
20. Z. G. Pinsker, *Dynamical Scattering of X-Rays in Crystals* (Nauka, Moscow, 1974; Springer, Berlin, 1978), p. 369.
21. V. A. Bazylev and N. K. Zhevago, *Radiation of Fast Particles in Materials and in External Fields* (Nauka, Moscow, 1987), p. 272 [in Russian].
22. G. Borrmann, Z. Phys. **42**, 157 (1941).

Translated by A. S. Betev